Broadband control of plate radiation using a piezoelectric, double-amplifier active-skin and structural acoustic sensing

Brody D. Johnson and Chris R. Fuller
Vibration and Acoustics Laboratories, Department of Mechanical Engineering, Virginia Polytechnic Institute and State University, Blacksburg, Virginia 24061

(Received 7 October 1998; accepted for publication 21 October 1999)

The potential of a piezoelectric, double-amplifier active-skin with structural acoustic sensing (SAS) is demonstrated for the reduction of broadband acoustic radiation from a clamped, aluminum plate. The active-skin is a continuous covering of the vibrating portions of the plate with active, independently controllable piezoelectric, double-amplifier elements and is designed to affect control by altering the continuous structural radiation impedance rather than structural vibration. In simulation, acoustic models are sought for the primary and secondary sources that incorporate finite element methods. Simulation indicates that a total radiated power attenuation in excess of 10 dB may be achieved between 250 and 750 Hz with microphone error sensing, while under SAS the radiated power is reduced by nearly 8 dB in the same frequency range. In experiment, the adaptive feed forward filtered-*x* LMS (least mean square) algorithm, implemented on a Texas Instruments C40 DSP, was used in conjunction with the 6I6O control system. With microphone error sensing, 11.8-dB attenuation was achieved in the overall radiated power between 175 and 600 Hz, while inclusion of SAS resulted in a 7.3-dB overall power reduction in this frequency band. © *2000 Acoustical Society of America.* [S0001-4966(00)00702-5]

PACS numbers: 43.55.Vn [PJR]

INTRODUCTION

Recent work in the areas of active noise control (ANC) and active structural acoustic control (ASAC) have shared a common trend: the pursuit of practical active control systems that may be applied in more generalized noise control environments. In such general environments, the necessary actuators and sensors must comply with predetermined space and weight requirements. Furthermore, the influence of the secondary system on the performance of the primary structure must also be considered in design. Example applications where such design issues are of prime concern arise in the automotive and aeronautical fields. In order to satisfy the constraints imposed in these and other applications, lightweight, compact, and robust control systems must be devised. This motive has led to the investigation of a wide variety of control approaches. One approach, discussed in this paper, consists of a complete covering of the radiating surface of a structure with a specially designed conformal skin. This skin may exhibit both passive and active characteristics and in many cases is comprised of a number of individual skin elements that make use of one or both of these tactics. In this approach one is concerned with sound radiated from the surface of the skin rather than the primary structure. Since the active-skin functions by modifying the radiation impedance, it is not necessary to directly modify the structural vibration and the approach is suitable for massive or stiff structures that have low mobility. The skin may also possess integrated sensing capabilities, such as structural acoustic sensing (SAS). SAS consists of the prediction of acoustic error from vibration information taken from a number of structurally mounted sensors. Maillard and Fuller have shown, both analytically and experimentally, that SAS is an effective technique for the estimation of an acoustic cost function in multichannel ASAC systems.[1,2]

An example of a passive–active skin, provided by Gentry, Guigou, and Fuller, is one that integrates a number of independent polyvinylidene fluoride (PVDF) actuators in a foam layer located on a vibrating piston.[3,4] This approach offers an increase in the low-frequency performance of the foam skin while still taking advantage of the passive properties of the foam at high frequency. For another skin approach, described in this paper, consider a primarily active-skin consisting of a number of independent skin cells, which are used to prevent radiation through the minimization of an acoustic cost function.[5] With this scheme, the skin cells must provide substantial control authority over the entire bandwidth of interest. Kugel and others have developed analytical models for the dynamic characterization of piezoelectric (PZT) acoustic transducers intended for use in an active-skin of this nature.[6]

Ross and Burdisso have also devised an interesting approach to the passive skin concept, by designing what is essentially a single degree of freedom (DOF) skin element.[7] When this passive device is applied to a vibrating surface, the mass component of the single DOF element is forced to vibrate at one level, while the base surrounding the mass element shares the original vibration level of the primary structure. Thus for frequencies above the resonance of this single DOF system, the mass and base elements vibrate out of phase. By determining the appropriate areas for the base and mass surfaces of the skin element, an acoustic dipole is created.

A number of examples of the skin concept in the control of sound were discussed in the previous paragraphs. In each of these examples the goal lies in the development of a com-

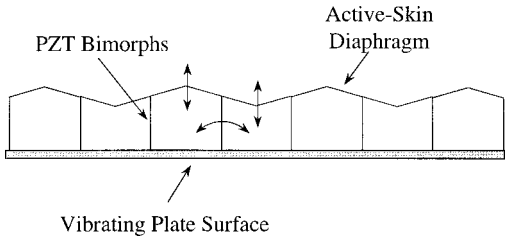

FIG. 1. The active-skin concept.

pact noise suppression system, albeit passive or active, that allows for application to a wider variety of noise control problems. It is such a system that will be evaluated here. The active-skin concept applied in this work is depicted in Fig. 1. By exciting the PZT bimorphs comprising the flexible leg elements of the active-skin, an amplified diaphragm response is obtained. The cell design employed here, shown in Fig. 2, provides two means of amplification of the acoustic response which are designed to provide a high level of diaphragm vibration with only a small space requirement. First, the use of bimorph PZT actuators, driven out of phase, provides an amplified flexural response of the legs of the cell. Since the cell legs are clamped at their base, the maximum leg displacement occurs at the joint between the legs and the cell diaphragm. By driving the two legs of a cell with opposite polarity, the diaphragm is forced to vibrate. Here the second stage of amplification is encountered as the response of the diaphragm tip is geometrically amplified with respect to the leg motion. The active-skin is then comprised of a number of these cells, each independently controllable. The independence of the individual cells provides the needed flexibility for attenuation of high-order modes, while also introducing the possibility of acoustic coupling between cells. This potential problem is handled by careful choices in error sensing and, in general, it is wise to use more error sensors than skin cells to prevent such interaction.

This work shall serve two main purposes. First, to develop a numerical model describing the active-skin system, as applied to plates, for investigation of the active-skin as a viable control approach in generalized structural radiation problems. Second, to verify the analytical findings by realizing the active-skin in experiment. The chosen primary structure is a clamped plate, which represents a building block common to many structures encountered in noise control applications, e.g., buildings, cars, machinery casings, etc.[8]

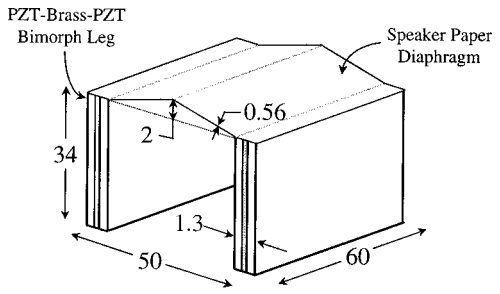

FIG. 2. The active-skin cell (dimensions in mm).

I. NUMERICAL ACTIVE-SKIN MODEL

In this section the numerical representation of the active-skin is introduced. The structural modeling techniques shall be discussed in the context of a single active-skin cell, as depicted in Fig. 2. This cell design makes use of bimorph PZT actuators on the legs of the cell and a light speaker paper material for the diaphragm. A description of the acoustic modeling approach follows, including the integration of SAS into the simulated error sensing. Once the necessary models are developed, a description of the control simulation is given. Finally, the setup of the virtual active-skin system is described, including the primary structure, skin cell, and error sensor locations.

A. Structural modeling

The IDEAS® finite element method (FEM) package was used for the creation of a 180-element, 210-node, representation of a single active-skin element.[9] A thin-shell element type was adopted for this model, providing six degrees of freedom (DOF) for each of the four nodes comprising an element. These DOF include translational motion along and rotational motion about the three coordinate axes. The element formulation also requires definition of the element thickness, mass density, modulus of elasticity, and Poisson's ratio for each element. For the purposes of this model, the materials are assumed to behave isotropically.

Having briefly introduced the FEM approach adopted in this analysis, a discussion of important mesh features will now be undertaken which pertain to the active-skin cell. First, as shown in Fig. 2, the bimorph PZT actuators are comprised of three layers of material, in which two 0.6-mm layers of PKI550 PZT sandwich a 0.1-mm layer of brass shim. The variation of material properties across this section is ignored for this model (along with the bonding layers), with PZT material properties assumed over the entire cross section. Similarity between the brass and PZT mechanical properties suggests that such an assumption should not significantly affect the modeling results. Second, three creased bends exist in the paper diaphragm of the active-skin cell. These bends, or hinges, are modeled by torsional springs, which act to impose resistance against the free rotation of the diaphragm about these creases. With this approach, the torsional stiffness may be tuned to match experimentally observed behavior. Clamped boundary conditions were assumed for nodes at the base of the PZT legs.

The simultaneous vector iteration approach is used to determine the mode shapes and resonant frequencies for the active-skin cell.[9,10] Each mode shape is expressed as a vector whose components represent the nodal displacements associated with a given mode. For such a multidegree of freedom system, the response to a harmonic input may be expressed as a summation over the orthogonal modes by

$$w(n,t)=\sum_{m=1}^{M} A_m \Phi_m(x,y)\sin(\omega t), \tag{1}$$

where w represents the displacement function, n refers to the nodal coordinate system, t is time, A_m is a complex modal amplitude, Φ_m is the mth mode shape, and ω is the excitation

frequency.[10] To determine the induced modal amplitudes for an arbitrary harmonic excitation, the assumed solution of Eq. (1) must be substituted into the transformed equation of motion, which reduces to

$$[\Phi]^T[M][\Phi]\{-\omega^2 A\}+[\Phi]^T[K][\Phi]\{A\}=[\Phi]^T\{F\}, \tag{2}$$

where Φ is the modal matrix, M is the mass matrix, K is the stiffness matrix, A represents the modal amplitude vector, and F is the nodal force vector. Further reduction of Eq. (2) yields the mth modal amplitude as

$$A_m=\frac{1}{m_d(\omega_m^2-\omega^2)}\{\Phi_m\}^T\{F\}, \tag{3}$$

where m_d is the normalization constant such that $\{\Phi_m\}^T[M]\{\Phi_m\}=m_d$, and ω_m is the natural frequency of the mth mode.

At this stage, it remains only to discuss the determination of a nodal force vector that appropriately represents the action of the piezoelectric actuators of the active-skin cell. The approach applied here was first proposed by Crawley and De Luis for the representation of one-dimensional piezoelectric actuators.[11] In 1991, Dimitriadis, Fuller, and Rogers developed an extension to two-dimensional scenarios, such as that encountered in this work.[12] The goal in the implementation of this model is to determine equivalent external edge moments to apply to the FEM models for characterization of the vibrational behavior of the active-skin cell. It should be noted that the approaches suggested in the references above do not directly apply here, due to the relative thickness of the piezoelectric material in the skin cell to the underlying structure. The models are used only to provide a more realistic loading of skin cell by application of the control voltage and, for purposes of simulation, are sufficient to meet this end.

B. Acoustic modeling

The objective of the acoustic modeling is to predict the far-field radiation from the active-skin. Since the skin may be effectively viewed as a baffled, planar radiator, it is the simple half-space radiation problem that requires attention. Under this limitation, the far-field radiated pressure depends only upon the normal surface velocity of the radiating structure. Each FEM element is treated as a component source of the complex radiating structure. When each of these component sources is small compared to the acoustic wavelength (maximum dimension $\ll\lambda$), the analysis will appropriately model the phase variation of the radiated pressure.[13] Thus under these assumptions, the pressure radiated to a point in the acoustic medium may be written in terms of Rayleigh's integral as

$$p(\vec{r})=\frac{j\omega\rho_0}{2\pi}\sum_S\left[\nu_n(\vec{r}_s)\frac{e^{-jk|r-r_s|}}{|\vec{r}-\vec{r}_s|}\right]dS, \tag{4}$$

where p is the observed acoustic pressure, ρ_0 is the density of the acoustic fluid, ν_n is the normal velocity, $\vec{r}$ is the position vector of the point at which the pressure is determined, and $\vec{r}_s$ is the position vector locating a surface element of the vibrating structure.[8]

From the FEM representation of a vibrating structure, the velocity of the structure at a number of defined nodal locations is known. Combining the nodal velocities with knowledge of the structure's geometry, the normal surface velocity may be computed for each element comprising the structure. This discretized normal surface velocity suggests that Rayleigh's integral must be approximated by a sum over the elements comprising the complex structure. This discretization takes the following form:

$$p(\vec{r})=\sum_{m=1}^{N}\frac{j\omega\rho_0}{2\pi}S_m\nu_m\frac{e^{-jkR_m}}{R_m}, \tag{5}$$

where the index m identifies an element of the vibrating structure, N is the total number of elements, S_m is the area of the mth element, ν_m is the normal velocity of the mth element, and R_m is the distance between the center of the mth element and the point in the acoustic medium at which the pressure is to be evaluated. As long as the maximum element dimension satisfies the above low-frequency assumption, a discretized evaluation of Eq. (4) will yield an accurate measure of the pressure radiated to desired points in the acoustic medium. Note that this method is most appropriately applied to planar, baffled radiators; however, when the size of a nonplanar source is small compared to the acoustic wavelength, it may also be represented in this manner.[13]

This modeling approach may also be modified for use in the study of structural acoustic sensing (SAS) with the active-skin. The basis of the SAS technique is that, for relatively simple geometries, the acoustic radiation may be predicted from a thorough knowledge of the surface velocity over a vibrating structure. In the previous paragraphs, a *complete* knowledge of this information was available, allowing for direct determination of the radiated pressure. The idea behind SAS is to accurately predict the radiated pressure from only a *partial* knowledge of the surface velocity field. As with the results in the previous paragraph, the radiated pressure will be expressed as a sum over a number of component radiators; however, here the component radiators will consist of a number of elements rather than one. In this work, the radiation from these areas is assumed to resemble a monopole, although an unlimited number of alternative pressure formulations may be assumed for the discretization.[1,2] For this model, the pressure estimate at a point in the acoustic medium may be written, in the frequency domain, as a summation of the accelerometer signals as

$$p(\vec{r})=\sum_{m=1}^{N}\frac{\rho_0}{2\pi}S_m a_m\frac{e^{-jkR_m}}{R_m}, \tag{6}$$

where the index m identifies an accelerometer of the SAS array, N is the total number of SAS sensors, S_m is the area of the radiating surface associated with the mth sensor, a_m is the normal acceleration at a point in the mth component area, and R_m is the distance between the mth sensor and the point in the acoustic medium at which the pressure is to be evaluated, which is defined by the position vector $\vec{r}$.

In order to implement SAS in real-time as a supplement to a time-domain feed forward algorithm, an array of digital filters modeling the various sensor paths is required.[1,2] The

appropriate digital filters necessary for modeling these transfer functions must be found using a numerical curve fit with a reasonable number of finite impulse response (FIR) filter weights. The difficulty in developing a practical SAS system lies in achieving an adequate representation of the acoustic radiation with a minimal number of structural sensors. These ideas will resurface below when SAS is applied in experiment with the active-skin.

C. Control simulation

In practice, the active-skin will be used as part of an adaptive control system making use of the filtered-*x* LMS feed forward algorithm.[14] In simulation it is impractical to mimic such an algorithm, prompting for an alternative means for time-domain evaluation of the control performance of the active-skin system. The method adopted in this work takes advantage of the quickness of a frequency-domain solution and the practicality of a time-domain approach. With this method, the optimal control compensator responses, $W(z)$, are determined in the frequency domain using linear quadratic optimal control (LQOC) theory.[15] This approach entails writing the quadratic cost function (a sum of the squared error) in terms of the disturbance and control inputs and subsequently determining the optimal control inputs which result in the minimization of this cost function. It is assumed in this analysis that the presence of the active-skin does not affect the acoustic radiation of the primary structure, limiting the analysis to the far-field control problem. Once the frequency responses have been isolated, the MATLAB® function INVFREQZ may be used to design digital filters for use in time-domain simulation.[16] This transformation uses a curve-fitting technique to provide the best possible *causal* representation (for a defined number of weights) of the desired complex frequency response. This transformation places a realistic limit on the performance of the control compensators, as found in experiment with a feed forward approach. Upon determination of the control compensators, an arbitrary time signal may be generated for the disturbance and fed through the primary and secondary control paths for evaluation of the control performance. Thus this hybrid approach to simulation entails the design of digital filters from frequency-domain transfer functions, along with the time-domain implementation of these filters with respect to a random disturbance, generated in MATLAB®.

D. Plate and active-skin coordinate systems

As mentioned earlier, in this work the active-skin is applied to a clamped, aluminum plate. The plate is rectangular, of dimensions $170\times150\times1.5$ mm, and is mounted in a baffle. A broadband disturbance is provided to the plate through a piezoelectric actuator ($38\times30\times0.1$ mm) located for effective excitation of the first six plate modes. The location of the disturbance actuator on the plate is shown in Fig. 3. The response of the plate is determined using a FEM approach analogous to that used with the active-skin cell. For brevity this model is not presented here, but let it be noted that the acoustic response of the plate is again determined from the structural response by means of Rayleigh's integral,

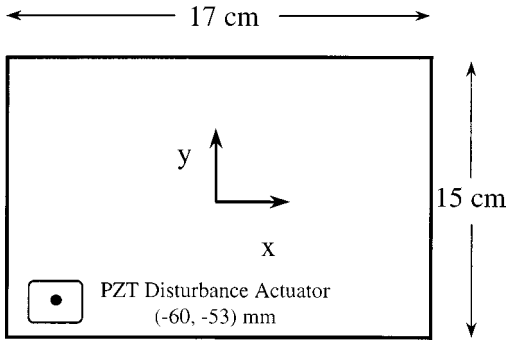

FIG. 3. The piezoelectric disturbance actuator.

which is evaluated in a discretized form. For the purposes of this work, the active-skin is mounted just above the surface of the plate, preventing vibrational coupling between the two structures. It is further assumed that the acoustic fields of these two structures may be determined separately and superposed for determination of the complete sound field. A typical configuration of the active-skin is represented by Fig. 4, with the origin of the coordinate system taken at the center of the plate.

In Sec. I C, the combined frequency-time-domain simulation approach was described. While a reference signal is not required for the frequency-domain determination of the optimal control compensator responses, a reference signal *is* necessary for the time-domain evaluation of these compensators under an arbitrary excitation. The ideal reference (the disturbance input) is assumed for this work. The error signals are sound pressure, measured or predicted (in the case of SAS) at a number of far-field locations. The sound pressure at a number of distinct observation points is also monitored for estimation of the global control performance. Both acoustic directivity and radiated sound power comparisons are made between the controlled and uncontrolled responses of the system.

II. NUMERICAL RESULTS

Three key results will be presented in this section. First, the tuned FEM model is presented and compared to experimentally measured resonant frequencies. Next, the complete active-skin model is used to demonstrate the effectiveness of this control approach in a 6I6O control system, which uses

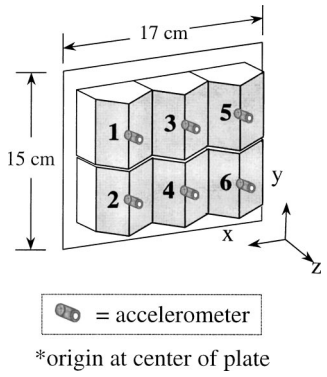

FIG. 4. 6I6O active-skin cell configuration.

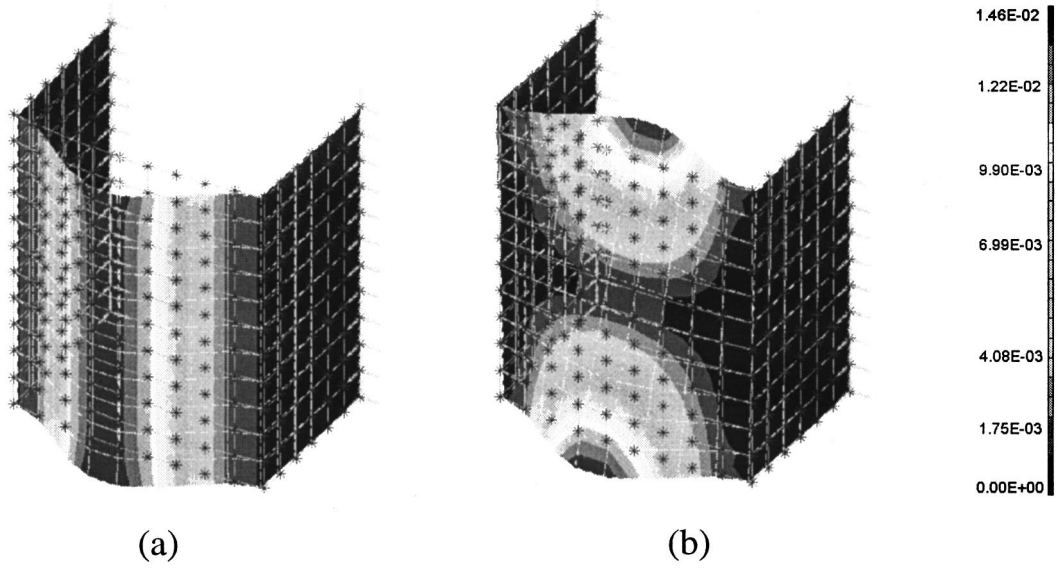

FIG. 5. Displacement magnitude: (a) first active-skin cell mode: 246 Hz (250 Hz) and (b) second active-skin cell mode: 374 Hz (390 Hz).

microphones as error sensors. Finally, an investigation of the effect of SAS on the active-skin is undertaken using the developed numerical model.

A. Structural modeling

The FEM approach to modeling the active-skin cell was outlined earlier in this paper. In order to tune the torsional springs used along the bends in the diaphragm of the active-skin cell, experiments were conducted in which the vibrational response of a single cell was observed for a broadband voltage excitation. In these experiments, a laser vibrometer was used to collect normal velocity data over the surface of the diaphragm. By computing the experimental frequency response function (FRF) relating the applied voltage to the cell vibration at various positions, the experimental modes and mode shapes of the active-skin cell were obtained. Only the first two modes made significant contributions to the observed response; therefore, it is the first two modes that will be presented here. Figure 5(a) displays the mode shape obtained from the FEM model for the first mode of the active-skin cell. Beneath this depiction, the FEM resonant frequency is given along with the experimentally observed value, the latter in parentheses. This mode dominates the frequency response except near the second resonance. Excitation of the first mode results in the desired diaphragm motion for efficient sound radiation. In Fig. 5(b), however, a less efficient radiating second mode is depicted. Here, the upper and lower halves of the diaphragm vibrate out of phase, resulting in reduced far-field radiation for low frequencies.

B. Microphone error sensing results

The first simulation performed with the active-skin is intended to show the potential of the secondary acoustic sources, the skin cells, for application to generalized structural radiation problems. Microphone error sensing is used to meet this end, before a more compact SAS sensing scheme is employed. Six cells are used for this embodiment of the active-skin, shown in Fig. 4. The accelerometers depicted in this figure are used only for simulation with SAS, below. the skin cells were distributed evenly over the surface of the plate and the microphones were positioned to sense all six radiating modes included in the analysis.

The time-domain portion of the simulation was performed with a sample rate of 1600 Hz, employing 96 coefficient FIR filters in the control path and 255 coefficient FIR filters serving as control compensators. This means that 255 FIR coefficients are used to model the optimal compensator frequency responses, as determined from LQOC theory. A target control bandwidth was chosen ranging from 250 to 750 Hz, encompassing six structural modes of the clamped aluminum plate. Figure 6 depicts the control performance in terms of the radiated sound power from the plate/skin system. An overall reduction in the acoustic power of 11.7 dB is observed between 250 and 750 Hz.

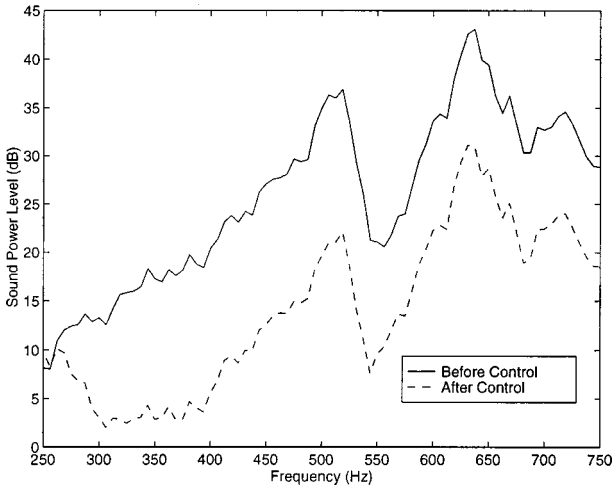

FIG. 6. Radiated acoustic power before and after control.

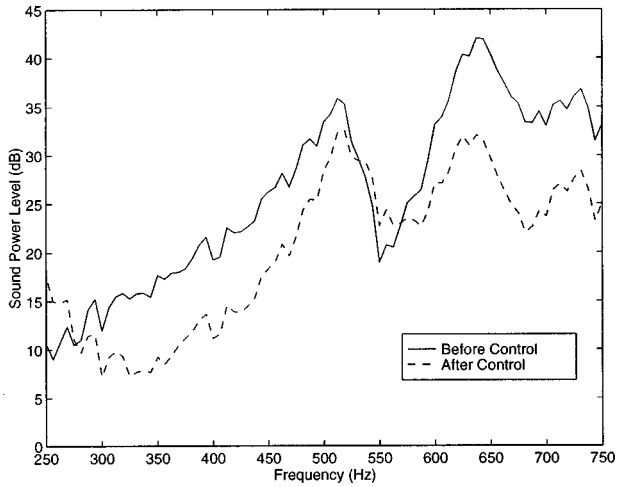

FIG. 7. Radiated acoustic power before and after control with structural acoustic sensing.

C. SAS error sensing results

Here, a SAS sensing scheme will be incorporated into the model of the previous section as a step toward a more practically realizable control system. The six active-skin cell locations from above were retained; however, an accelerometer is positioned at the center of the diaphragm of each skin cell, as depicted in Fig. 4. These sensors provide the structural information necessary for prediction of the acoustic error signals.

In order to isolate the effect of SAS on the control performance of this system, the simulation parameters from the previous control configuration are retained here. A comparison between the SAS-predicted and the analytically determined transfer functions relevant to the system was made prior to simulation. Only minor phase error (at high frequency) was evident from this comparison, suggesting that the SAS system provides an adequate model of both the control-to-error and disturbance-to-error paths. Implementation of this SAS active-skin system yields a 7.9-dB reduction in the overall sound power radiated from the plate/skin system. The radiated sound power frequency spectra for this simulation are shown in Fig. 7, respectively.

III. EXPERIMENTAL ACTIVE SKIN

Before presenting experimental results achieved with the active skin, it is necessary to first discuss the means for practical implementation of the active skin and the SAS error sensing technique. As mentioned above, the adaptive feed forward filtered-*x* LMS algorithm is applied through the use of a digital signal processor (DSP). Familiarity with algorithms of this nature shall be assumed and the unfamiliar reader is referred to the literature.[14,17,18] In the absence of far-field microphone error sensing, a second DSP is used to implement the SAS sensing scheme. Previous work with SAS has relied on the known radiation behavior of specialized geometries, while in this work a convenient experimental technique is used to determine relationships between the measured structural vibration and the desired far-field acoustic response. After a discussion of the application of SAS, the experimental setup will be introduced, which includes an improved skin cell design relative to that used in the numerical study.

A. Structural acoustic sensing in experiment

This section is devoted to the development of an experimental methodology for the prediction of the radiated acoustic pressure using a number of accelerometers, which are distributed over the radiating surfaces of the active skin. The accelerometer signals are used in conjunction with an array of specially designed digital filters to construct signals corresponding to the acoustic pressure at desired points in the far-field. For accurate prediction of the acoustic error, the influence of a given structural response on the acoustic pressure at a desired error location must be known. As discussed above, this relationship between the structural sensors and the error locations may be found using analytical methods. Alternatively, it is possible in some instances to measure the relationships directly. One way to do this is to excite each isolated area of the radiating surface independently, measuring the desired frequency response functions (FRF's) in the process. Fortunately, the individual skin cells of the active-skin provide a convenient means for the isolation of these influence functions. Thus the desired influence relationships are determined by exciting a single skin cell and directly measuring the transfer functions between an accelerometer mounted on the cell to each of the far-field microphones. This process yields the necessary information for relating the skin vibration to the measured acoustic response in the far-field, but fails to characterize the relationship between the plate vibration and the associated far-field acoustic disturbance. By placing a single additional accelerometer on the plate and issuing a disturbance to the plate via a shaker, a similar set of measurements may be made which characterizes the effect of the plate vibration on the net error. It is important to note that any ''cross-talk'' between the structural sensors would serve to dissolve the validity of this approach. This coupling is eliminated by mounting the skin cells on a perforate sheet (acoustically transparent) slightly above the surface of the plate. Once the influence functions have been determined, they must be incorporated into a real-time DSP code. Thus an array of digital filters modeling the various sensor paths is required.

B. Experimental setup

A rough schematic of this skin cell design is given in Fig. 8(a). In this sketch, the dashed lines depict an exaggerated motion of the skin cell frame, while solid black lines represent the motion of the diaphragm. This improved cell design includes piezoelectric material inside the frame, with an outer covering of steel for protection of the piezoelectric material. A stiff, lightweight carbon–graphite material is used for the diaphragm, preventing high-order diaphragm modes from dominating the response of the device. The actual devices used for this experimentation were designed and fabricated by the Material Research Laboratory at the Pennsylvania State University at State College, Pennsylvania.[6] One such device, which is approximately $55\times55\times20$ mm in size, is shown in Fig. 8(b). In this most recent design, the

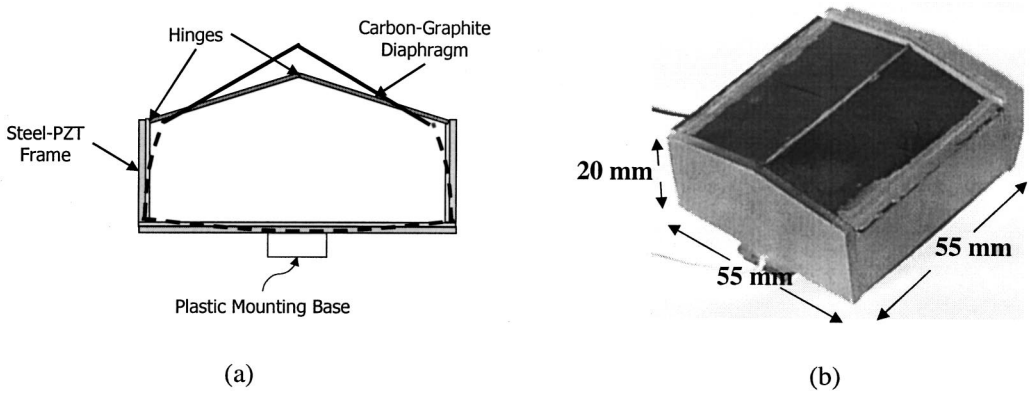

FIG. 8. The active-skin cell design: (a) schematic and (b) a single active-skin cell.

additional piezoelectric material employed on the bottom of the skin cell allows for even greater displacement of the cell diaphragm. Again, the active skin is implemented on a clamped, aluminum plate of dimensions $170\times150\times1.5$ mm. The plate is mounted in a baffle inside an anechoic chamber ($4.2\times2.5\times2.2$ m). A tubular hemisphere was used to support a number of microphones and a traverse boom was used to acquire in-plane acoustic directivity data over the 180°-space on the front side of the baffle. Sixteen microphones were mounted on the hemisphere, six for use as error sensors in microphone sensing configurations and an additional ten to provide a picture of the total radiated acoustic power. Note that each of these ten locations is distinct from the microphone error sensor locations. A schematic of the experimental setup is given in Fig. 9. Dashed lines are used with the microphones to indicate that either microphone or SAS sensing is adopted for a particular control configuration. As depicted in Fig. 9, a shaker mounted to the plate from the backside of the baffle disturbs the plate. The skin cells are mounted to a perforated aluminum support plate approximately 5 mm in front of the surface of the plate. An accelerometer is mounted to each radiating structure, one on each of the six skin cells and another on the backside of the plate. The signals from each accelerometer are passed along to the SAS filter DSP, see Fig. 9, where the SAS filtering is performed on a TI-C30 DSP. Thirty coefficients are employed in each of the 42 SAS paths at a 1300-Hz sample rate. A TI-C40 DSP is used to implement the filtered-*x* control algorithm at a sample rate of 2000 Hz, accepting error signals from the SAS filter DSP. With this sample rate, the control compensators and system identification filters may possess up to 175 and 96 FIR coefficients, respectively. The ideal reference (the disturbance input) is used in this work. The maximum filter length is applied in each control configuration. The limiting factor in the controllable bandwidth of this application of the active skin is the 1300-Hz sample rate of the SAS sensing. Hence, all control experiments are conducted for a band-limited random disturbance between 175 and 600 Hz to ensure accurate prediction of the far-field acoustic error.

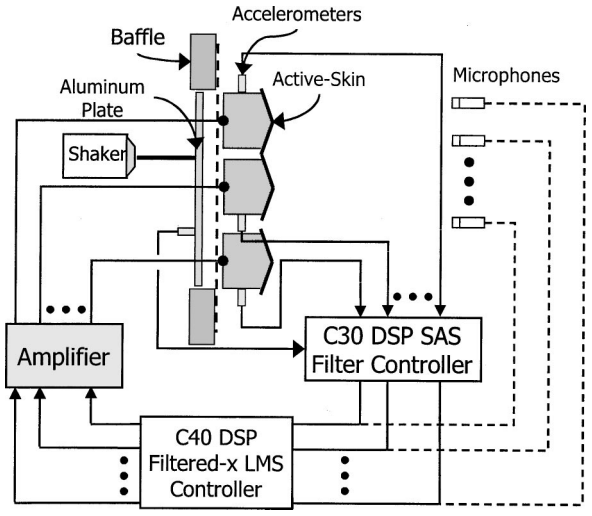

FIG. 9. The active-skin experimental setup.

IV. EXPERIMENTAL RESULTS

The primary objective of this work is to show the potential of the active-skin in the control of structural radiation; however, a secondary objective is to demonstrate the utility of such a skin in tandem with SAS. Thus the skin is employed first with far-field microphones serving as error sensors and second with the integration of SAS. The six-cell active-skin, mounted to a perforated aluminum sheet, is depicted in Fig. 10, showing the accelerometers mounted at the center of the diaphragm of each cell. Note that a seventh structural sensor is located on the backside of the aluminum plate. The following paragraphs summarize the results ob-

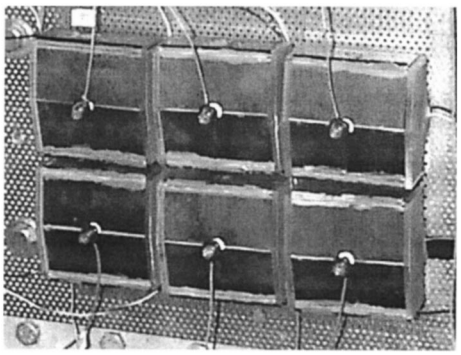

FIG. 10. The active-skin in a top-mounted structural acoustic sensing configuration.

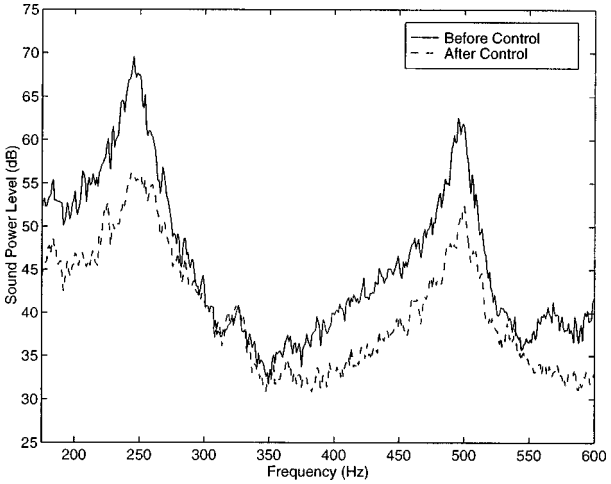

FIG. 11. Radiated sound power spectra, top-mounted accelerometer configuration with microphone sensing.

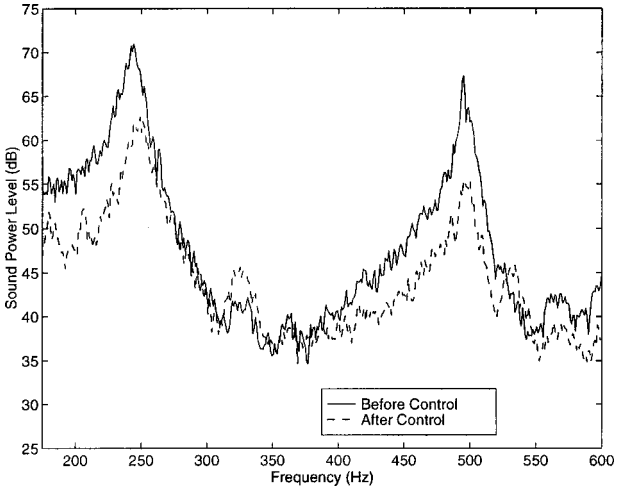

FIG. 12. Radiated sound power spectra, top-mounted accelerometer configuration with structural acoustic sensing.

tained for this mounting configuration under the aid of microphone and SAS sensing systems, respectively.

To set the pace for the SAS system, the microphone sensing setup is adopted first. For this 6I6O control system, the error microphones were distributed evenly over the tubular hemisphere described above. The shaker attached to the plate was driven with band-limited random noise between 175 and 600 Hz. While several plate modes are present in the frequency range investigated, the response of the plate is dominated by two modes due to the nature of the shaker loading. The filtered-*x* algorithm was employed with a sample rate of 2000 Hz and 175 coefficients were used in each of the six adaptive FIR control compensators. Following a three-minute period of system identification, the control compensators were allowed to adapt for two minutes. An estimate of the radiated sound power is given in Fig. 11 for the controllable bandwidth, which reveals significant attenuation around each resonant frequency of the aluminum plate. An impressive 9.5-dB reduction is achieved in the controlled power radiation from the plate-skin system in the 175- to 600-Hz bandwidth.

Having established a baseline performance for the active-skin, the primary objective of this work, as discussed above, is satisfied. The SAS system shall now be included to predict the acoustic error at each of the microphone locations used in the previous experiment. The 42 influence paths, relating the seven structural signals to each of the six error estimates, were obtained using the experimental procedure outlined in Sec. III A of this work. Once these paths have been identified, a straightforward application of the control algorithm is made. Again, a sample rate of 2000 Hz was used, in conjunction with 175 coefficient adaptive control compensators. A 1300-Hz sampling frequency was adopted with the SAS controller, using 30 coefficients in each of the SAS influence paths. A total radiated power reduction of 7.3 dB was attained over the 175 to 600 Hz bandwidth. The corresponding frequency spectra are given in Fig. 12.

V. CONCLUSIONS

In this work, both numerical and experimental methods were used to demonstrate the effectiveness of a piezoelectric double-amplifier active-skin in conjunction with SAS for the control of broadband radiation from a clamped, aluminum plate. A comparison between SAS and traditional sensing arrangements was made in both the numerical and experimental studies in order to validate the practically of an active-skin approach to systems where far-field microphone error sensing is impractical. FEM techniques were used to develop a structural model of a single active-skin element, which was, in turn, applied to the numerical determination of the acoustic radiation from this source. Integration of this structural-acoustic model into a combined frequency- and time-domain control approach led to the numerical evaluation of the 6I6O active-skin system. Numerical results indicate that the total radiated sound power may be reduced by as much as 11 dB using microphone sensing and by nearly 8 dB using SAS. In experiment, microphone error sensing led to an approximate attenuation of 10 dB in the total radiated sound power, while SAS error sensing yielded roughly a 7-dB attenuation. Significant attenuation in radiated sound power was achieved with each active-skin configuration. While the SAS configurations resulted in a lessened control performance with respect to the corresponding microphone sensing result, substantial reduction was still obtained. This degradation of control performance is suspected to depend on the maximum sample rate and filter lengths attainable with the SAS filter DSP. These results further suggest that the active-skin system is conducive to the inclusion of SAS, which makes the actuator-sensor system more compact and, hence, more practical than many previously developed ASAC or ANC systems.

The main conclusion drawn from this work is that the piezoelectric, double-amplifier active-skin system shows potential for application to broadband structural radiation problems, including those where far-field microphone sensing would represent an impractical error sensing scheme and when the radiating structure is relatively massive.

ACKNOWLEDGMENT

The authors gratefully acknowledge the funding of this research under Grant No. N00014-94-1-1140 by the Office of Naval Research, Dr. Kam Ng, Technical Monitor.

[1] J. Maillard and C. R. Fuller, ''Advanced time domain wave-number sensing for structural acoustic systems, Part I: Theory and design,'' J. Acoust. Soc. Am. **95**, 3252–3261 (1994).
[2] J. Maillard and C. R. Fuller, ''Advanced time domain wave-number sensing for structural acoustic systems, Part III: Experiments on active broadband radiation control of a simply-supported plate,'' J. Acoust. Soc. Am. **98**, 2613–2621 (1995).
[3] C. A. Gentry, C. Guigou, and C. R. Fuller, ''Smart foam for applications in passive/active noise radiation control,'' J. Acoust. Soc. Am. **101**, 1771–1778 (1997).
[4] C. A. Gentry, C. Guigou, and C. R. Fuller, ''Foam-PVDF smart skin for active control of sound,'' Proceedings of the 1996 Smart Structures and Materials Symposium, Industrial and Commercial Applications of Smart Structures Technologies, San Diego, California, Vol. 2721, pp. 26–37, February 1996.
[5] C. R. Fuller and B. D. Johnson, ''Control of structural radiation with an integrated piezoelectric double-amplifier skin,'' presented at the 1997 ONR Transducer Materials and Transducers Work Shop, State College, PA, April 1997.
[6] B. Xu, Q. M. Zhang, V. D. Kugel, W. Qingming, and L. E. Cross, ''Optimization of bimorph based double amplifier actuator under quasistatic situation,'' ISAF'96, Proceedings of the Tenth IEEE International Symposium on Applications of Ferroelectrics, 1996, Vol. 1034, p. 2; Vol. 1, pp. 217–220.
[7] B. W. Ross and R. A. Burdisso, ''Low frequency passive noise control of a piston structure with a weak radiating cell,'' J. Acoust. Soc. Am. **106**, 226–232 (1999).
[8] F. Fahy, *Sound and Structural Vibration* (Academic, London, 1985), Chap. 2, pp. 60–72.
[9] *I-DEAS Master Series User Guide Level 4: Model Solution and Optimization* (Structural Dynamics Research Corporation, Milford, Ohio, 1988), Chap. 6, pp. 6–7.
[10] L. Meirovitch, *Elements of Vibration Analysis*, 2nd ed. (McGraw-Hill, New York, 1975), Chap. 4, pp. 178–185.
[11] E. F. Crawley and Javier de Luis, ''Use of piezoelectric actuators as elements of intelligent structures,'' AIAA Paper 86-0878, pp. 1373–1385, October 1987.
[12] E. K. Dimitriadis, C. R. Fuller, and C. A. Rogers, ''Piezoelectric actuators for distributed vibration excitation of thin plates,'' Trans. ASME, J. Vib. Acoust. **113**, 100–107 (1991).
[13] L. E. Kinsler, A. R. Frey, A. B. Coppens, and J. V. Sanders, *Fundamentals of Acoustics*, 3rd ed. (Wiley, New York, 1982), Chap. 8, pp. 167–169.
[14] B. J. Widrow and S. D. Stearns, *Adaptive Signal Processing* (Prentice-Hall, Englewood Cliffs, NJ, 1985), Chap. 6, pp. 99–116.
[15] B. D. Johnson, ''Control of broadband structural radiation from structures using a piezoelectric double-amplifier active-skin,'' M.S. thesis, Department of Mechanical Engineering, Virginia Polytechnic Institute and State University, 1997.
[16] Mathworks, Inc., *MATLAB Signal Processing Manual* (Prentice-Hall, New York, 1995), Chap. 6, pp. 180–182.
[17] J. S. Vipperman, R. A. Burdisso, and C. R. Fuller, ''Active control of broadband structural vibration using the LMS adaptive algorithm,'' J. Sound Vib. **166**(2), 283–299 (1993).
[18] S. J. Elliot, P. A. Nelson, and I. M. Stothers, ''A multiple error LMS algorithm and its application to the active control of sound and vibration,'' IEEE Trans. Acoust., Speech, Signal Process. **35**, 1423–1434 (1987).